CYCLIC OXIDATION OF SINGLE-CRYSTAL NIAL-X ALLOYS

James A. Nesbitt, Charles A. Barrett,
NASA Glenn Research Center
Cleveland, OH 44135

Ram Darolia
General Electric Aircraft Engines
Cincinnati, OH 45215

ABSTRACT

Several single-crystal NiAl-X alloys (X=Hf, Ti, Cr, Ga) were cyclically oxidized at 1100°C for up to 1000 1-hr cycles. The alloys all showed protective, adherent α-Al_2O_3 scale formation with positive weight change behavior throughout the test. There was no clear correlation between the composition of the various alloys and the specific weight gain although the ranking by weight change was relatively consistent for two duplicate series of samples. The presence of Hf (0.5-0.8 at.%) resulted in the internal formation of Al_2O_3/HfO_2 "stringers." Diffusion of Hf to the growing oxide stringers resulted in the development of a near-surface layer depleted of these precipitates.

INTRODUCTION

Single-crystal nickel aluminide (i.e., β phase NiAl) has been under considerable investigation this decade as a potential structural material in aero gas turbine engines. The attractive features of NiAl in comparison to Ni-base superalloys include a higher melting point, lower density, higher thermal conductivity and excellent oxidation resistance.[1] However, NiAl suffers from a lack of ductility and fracture toughness at low temperatures, and low creep strength at high temperatures. These physical and mechanical properties have recently been reviewed in detail elsewhere.[2,3] Alloying additions of Hf, Ga, Ti and Cr have each shown significant benefit to the mechanical properties over that of the binary alloy.[4] However, the collective effect of these alloying additions on the environmental resistance of NiAl-X was unclear. Hence, the purpose of the present study was to examine the oxidation behavior of these alloys during thermal cycling (i.e., cyclic oxidation). A companion study was also undertaken to examine the hot corrosion resistance of these alloys.[5]

Numerous studies of the oxidation resistance of NiAl and its alloys have been performed over the past several decades due, in part, to the extensive application of aluminide coatings on high-temperature gas turbine components. Several studies have examined the effect of Al content on both the isothermal and cyclic oxidation behavior.[6-9] More recent ^{18}O/SIMS, TEM and STEM studies have examined the growth mechanisms of Al_2O_3 scales grown on binary alloys and alloys containing reactive element (RE) additions.[10-12] It is also well known that small additions of reactive elements, such as Zr, Y or Hf, to numerous high temperature alloys significantly improves the protective oxide

OK, Though why introduce an acronym used only twice?

OK

scale adherence during thermal cycling. However, an excessive RE addition can be detrimental, resulting in extensive internal oxidation in the form of oxide stringers or pegs. The extent of this stringer formation is directly related to the level of the RE addition, such as has been shown for Zr additions to NiCrAl[13,14] and NiAl alloys.[15]

EXPERIMENTAL PROCEDURE AND RESULTS

Eight single-crystal NiAl alloys were cyclically oxidized at 1100°C. All material was supplied by GEAE in a heat treated, hot isostatic pressed (HIP'ed) and aged condition. Details of this heat treatment are given elsewhere.[16] All single-crystal alloys received from GEAE contained Si as an impurity due to reaction of the NiAl alloy with the alumina-silicate mold. In addition, Zr was also found as an impurity traceable to the starting Hf material.[17] Alloy designations and compositions are given in Table I. Coupons were machined into approximately 1.3 cm diameter by 0.2 cm disks by wire EDM without regard to crystal orientation. A small hangar hole (0.15 cm diameter) was also machined into each coupon. The coupons were electrochemically etched in a perchloric solution to remove the EDM recast layer. Coupons were finally ultrasonically cleaned with acetone and ethanol.

Samples were examined using optical microscopy, scanning electron microscopy (SEM), energy dispersive spectroscopy (EDS), wavelength dispersive spectroscopy (WDS) and x-ray diffraction (XRD). WDS was used to resolve the peak overlap which occurs with EDS analysis of Hf and Si. For optical microscopy, samples were etched with a molybdic acid etch (50-75 ml HF, 150 ml H_2O, and 100 gm molybdic acid).

Initial Alloy Microstructures: Each of the alloy microstructures contained small oxide, carbide and intermetallic precipitates similar to the microstructures previously observed in NiAl-Hf-X alloys.[17-19] The etched microstructure of D218 (Fig 1) showed relatively large (~1 μm) precipitates, most likely either NiHfSi or Ni_2Al(HfTi) (Heusler) phase,[17,18] whose volume fraction varied significantly within the same sample. The precipitates in the high-Ti alloys (4-5%Ti) were much finer and more difficult to optically resolve, but also appeared to align along certain crystallographic planes (Fig 2a,b). This alignment is also apparent in the SEM micrographs shown in Fig 2c,d. Hf-rich oxides and carbides were also observed (Fig 3). EDS and WDS spectra of the carbides indicated that some of the carbides contain only Hf while other particles consist of mixes of both Hf and Ti. These observations are in agreement with the earlier TEM studies where both HfC and (Hf,Ti)C were observed.[19]

The alloys with higher Ti contents (3.9-5.4%) also contained large Hf-rich, three-phase regions consisting of primary Heusler, NiAl and NiHfSi (Fig 4). These regions are probably the remains of Hf-rich interdendritic regions observed in as-cast microstructures.[17,19] The bright phase within the Heusler phase, consisting of Ni, Ti, Hf,

Si and Zr, appears to be NiHfSi, although the presence of Ti is unclear. The Zr content was often significantly lower in other similar particles. Small amounts of NiAl (dark phase) are also present within the Heusler phase. Porosity was occasionally associated with these three-phase regions, in agreement with earlier studies.[19]

Cyclic Oxidation Testing: The coupons were tested in cyclic oxidation rigs at the Glenn Research Center.[20] Each cycle consisted of 1 hour at 1100°C in air followed by a cooling period of at least 20 minutes in ambient room air. Coupons were periodically removed from the furnace and weighed. The specific weight change through 500 and 1000 cycles is shown in Fig 5. Also shown in Fig 5b are typical weight changes for polycrystalline Ni-46.6Al and Ni-48.3Al-0.1Zr alloys.[9] The weight change for each of the single-crystal NiAl alloys increased through 1000 cycles indicating good scale adherence. Although the ranking by weight between the coupons tested for 500 and 1000 cycles was similar, there was no clear correlation between the weight change and the alloy composition (Fig 6). X-ray diffractometry of most samples after 100, 200, 500 and 1000 cycles showed primary formation of α-Al_2O_3 and HfO_2. A single small peak indicating the presence of TiO_2, was sometimes detected.

Post Test Alloy Microstructures: The fine precipitates present after the HIP and aging treatment in the high-Ti alloys (Fig 2) coarsened in regions away from the sample surface. EDS examination of these precipitates indicated the Heusler phase. In contrast, the precipitates initially present in D218 (Fig 1) had dissolved after 500 cycles indicating that either the particles initially present in D218 were not Heusler phase, or that the Heusler phase in D218, which contains less Ti, is not as stable as in the other alloys, in agreement with other recent studies.[21]

The typical oxide scale for each of the alloys consisted of a dense, continuous outer oxide layer above an inner region of oxide "stringers" penetrating into the alloy (Fig 7). At times, these oxide stringers showed considerable penetration into the sample (Fig 7b). The scale generally thickened with time (Figs 7c-f), but because of the very nonplanar nature of the scale, no attempt was made to quantify the rate of scale growth. There were also significant variations in the oxide penetration on the same sample, as can be seen by comparing Figs 7a with b, c with d, and e with f. These variations in the oxide stringer penetration are believed to be due to compositional inhomogeneities in the samples.

The outer oxide is shown at higher magnification in Fig 8. The dark oxide is Al_2O_3 and the brighter oxide is HfO_2. Typically, the oxide stringers growing into the alloy showed HfO_2 cores surrounded by Al_2O_3, with HfO_2 especially prevalent near the inner ends of the stringers. Al in the metal near the oxide/metal interface was somewhat depleted in comparison to that farther within the alloy (Fig 8) although etched samples did not reveal any γ'-$Ni_3(Al,Ti)$ formation near the surface. The less-reactive Ti in the

metal near the oxide/metal interface was also enriched as Al was selectively oxidized.

Large oxide formations indicating both inward and outward oxide growth were occasionally observed at the surface (Fig 9). EDS examination of these formations indicated a mixture of HfO_2 (brightest), TiO_2, NiO (medium gray) and Al_2O_3 (darker gray). These formations appear to result from the oxidation of the large, three-phase regions consisting of the Heusler, NiHfSi and NiAl phases (see Fig 4) located at the surface. Oxidation resulted in a near-surface depletion of the Heusler precipitates in the high-Ti alloys (Fig 10). The thickness of the depleted layer varied significantly within a single coupon, most likely due to inhomogeneity in the samples.

DISCUSSION

There was no clear correlation between the composition of the NiAl-Hf-X alloys and the specific weight gain. Since the stringer growth is a consequence of the presence of Hf, it was expected that A-26, the only alloy with a slightly higher Hf content (0.77%) would exhibit the highest weight gain. However, D218 exhibited the highest weight gain (Fig 5a). The high weight gain by D218 was unexpected since this alloy possesses the highest Al content (49.7%) and lowest Ti content (1%) which would seemingly result in less initial transient oxidation and therefore lower weight gains.

The weight change of the single-crystal NiAl-X alloys was not only positive, but exceeded, by up to a factor of two, the weight gain of the NiAl-0.1Zr alloy (Fig 7). A close examination of Figure 7 indicates that the higher weight gain of the NiAl-X alloys can be primarily attributed to oxide formation at shorter times (<50 cycles). Consequently, a portion of the increased weight gain can be attributed to transient oxidation of the additional alloying elements (Hf, Ga, Ti, Cr) in the NiAl-X alloys prior to the establishment of a continuous Al_2O_3 scale. In addition, optical micrographs of the NiAl-0.1Zr alloy after 3000 1-hr cycles at 1150°C[9] show little internal oxide formation in contrast to the significant stringer formation in the NiAl-X alloys. Hence, the higher weight gain of the NiAl-X alloys can also be attributed to the extensive stringer formation.

Stringer formation has been attributed to the selective oxidation of the reactive element within an alloy (eg., Y , Zr or Hf) enabled by the rapid transport of oxygen inward through the oxygen-deficient, reactive-element oxide.[22,23] Oxygen transport within these reactive-element oxides is several orders of magnitude greater than that for Al_2O_3.[24] In the present study, it appears that stringer formation occurs by diffusional transport of Hf to the growing stringers resulting in the depletion of the Hf-rich Heusler precipitates from the near surface region. The depletion of the Hf produces conditions sufficient for the oxidation of Al. Hence, Al oxidizes to form a case around the HfO_2 cores, significantly reducing radial growth of the HfO_2 stringers. It is clear that even after

1000 cycles, the Al_2O_3 has not totally encased the innermost tips of all of the stringers. The deep penetration of the oxide stringers observed in the present study could potentially degrade mechanical properties, such as fatigue.

CONCLUSIONS

The single-crystal NiAl-X alloys examined in this study exhibited excellent cyclic oxidation behavior, forming primarily protective α-Al_2O_3 scales. The high Hf content resulted in the internal formation of Al_2O_3/HfO_2 "stringers". There was no clear correlation between the composition of the various alloys and the specific weight gain although the ranking by weight change was relatively consistent for two series of samples.

REFERENCES

1. R. Darolia, JOM, **43**, p. 43, 1991.
2. R.D. Noebe, R.R. Bowman, and M.V. Nathal, "Review of the Physical and Mechanical Properties and Potential Applications of the B2 Compound NiAl," NASA TM 105598, April 1992.
3. D.B. Miracle, Acta. Metall. Mater., **41**, 649, 1993.
4. W.S. Walston, R.D. Field, J.R. Dobbs, D.F. Lahrman and R. Darolia, "Microstructure and High-Temperature Strength of NiAl Alloys," in *Structural Intermetallics*, R. Darolia, J.J. Lewandowski, C.T. Liu, P.I. Martin, D.B. Miracle and M.V. Nathal, editors, TMS, Warrendale, 1993, p. 523-532.
5. J.A. Nesbitt, "Hot Corrosion of Single-Crystal NiAl-X Alloys," NASA TM 113128, May 1998.
6. J. Doychak, J.L. Smialek, and C.A. Barrett, "The Oxidation of Ni-Rich Ni-Al Intermetallics," in *Oxidation of High-Temperature Intermetallics*, T. Grobstein and J. Doychak, editors, TMS, Warrendale, 1988, p. 41-56.
7. B.A. Pint and L.W. Hobbs, Ox Met., **41**, 203, 1994.
8. J.A. Nesbitt and C.A. Barrett, "Predicting the Oxidation-Limited Lifetime of β NiAl," in *Structural Intermetallics*, R. Darolia, J.J. Lewandowski, C.T. Liu, P.I. Martin, D.B. Miracle and M.V. Nathal, editors, TMS, Warrendale, 1993, p. 601-609.
9. C.A. Barrett, Ox. Met., **30**, 361, 1988.
10. E. Schumann, J.C. Yang, M. Rühle, M.J. Graham, Ox. Met., 46, 37, 1996.
11. R. Prescott, D.F. Mitchell, M.J. Graham and J. Doychak, Corr. Sci., 37, 1341, 1995.
12. B.A. Pint, J.R. Martin, and L.W. Hobbs, Ox. Met., **39**, 167, 1993.
13. C.A. Barrett, A.S. Khan, and C.E. Lowell, J. Electrochem. Soc., **127**, 670, 1980.
14. A.S. Khan, C.E. Lowell, and C.A. Barrett, J. Electrochem. Soc., **128**, 25, 1981.
15. J.A. Nesbitt, C.A. Barrett, J. Doychak, and E.J. Vinarcik, "Oxidation and Diffusional Transport in β-NiAl Alloys", HiTemp Review 1990, NASA CP 10051,

Paper 18, 1990.
16. J.A. Nesbitt, "Cyclic Oxidation of Single-Crystal NiAl-X Alloys," NASA TM 107346, December 1996.
17. I.E. Locci, R.M. Dickerson, A. Garg, R.D. Noebe, M.V. Nathal, and R. Darolia, "Microstructure and Phase Stability of Single Crystal NiAl Alloyed with Hf and Zr," Accepted for publication in J. Materials Research, **11**, Dec. 1996.
18. A. Garg, R.D. Noebe and R. Darolia, "Characterization of the Microstructure of a Hf-Doped NiAl Single Crystal Alloy Containing Different Levels of Si Contaminant," HiTempReview, 1995, NASA CP 10178, Paper 28, 1995.
19. R.D. Noebe, P.O. Dickerson, A. Garg, "Hierarchial Characterization of the Microstructure of Single Crystal NiAl Alloy AFN12," NASA TM 107029, 1995.
20. C. A. Barrett and C.E. Lowell, J. Testing and Eval., **10**, 273, 1982.
21. A. Garg, R.D. Noebe, J.M. Howe, A.W. Wilson and V. Levit, "TEM Study of Precipitation in a NiAl-3Ti-0.5Hf Single-Crystal Alloy," presented at *Microscopy and Microanalysis '96*, Minneapolis, MN, Aug. 11-15, 1996.
22. J.K. Tien and F.S. Pettit, Met. Trans., **3**, 1587, 1972.
23. H. Hindam and D.P. Whittle, Ox. Met., **18**, 245, 1982.
24. Per Kofstad, *High Temperature Corrosion*, Elsevier Applied Science, New York, 1988.

Table I.
Alloy Designations and Compositions (at.%)

Alloy	Ni	Al	Hf	Ga	Ti	Cr	Si
D218	48.5	49.7	0.51	0.12	1.0	0.0	0.15
D219	48.2	45.4	0.57	0.19	5.4	0.0	0.32
A-19	51.5	41.3	0.59	0.2	4.8	0.9	0.65
A-20	51.4	42.8	0.58	0.06	4.8	0.0	0.32
A-21	51.5	42.4	0.58	0.13	4.4	0.8	0.32
A-22	51.4	42.8	0.58	0.13	3.9	0.9	0.32
A-23	51.5	41.7	0.61	0.13	4.1	1.7	0.32
A-24	51.3	42.3	0.56	0.04	4.8	0.8	0.16
A-25	51.3	42.6	0.58	0.04	4.4	0.8	0.32
A-26	51.5	42.4	0.77	0.13	4.0	0.9	0.32

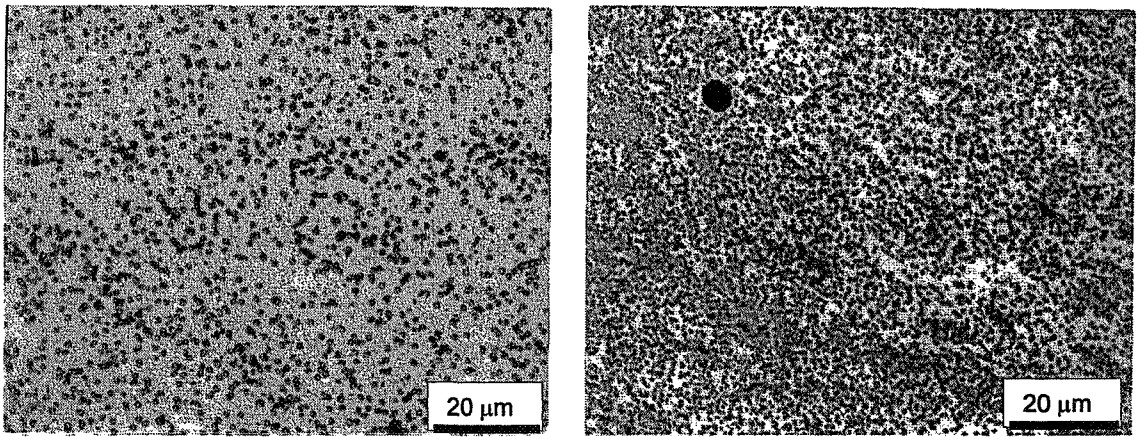

Figure 1. Optical micrographs showing the variation in volume fraction of the precipitates in the same etched sample of D218 (Ni-49.7Al-0.51Hf-0.2Ga-1.0Ti-0.15Si) before testing.

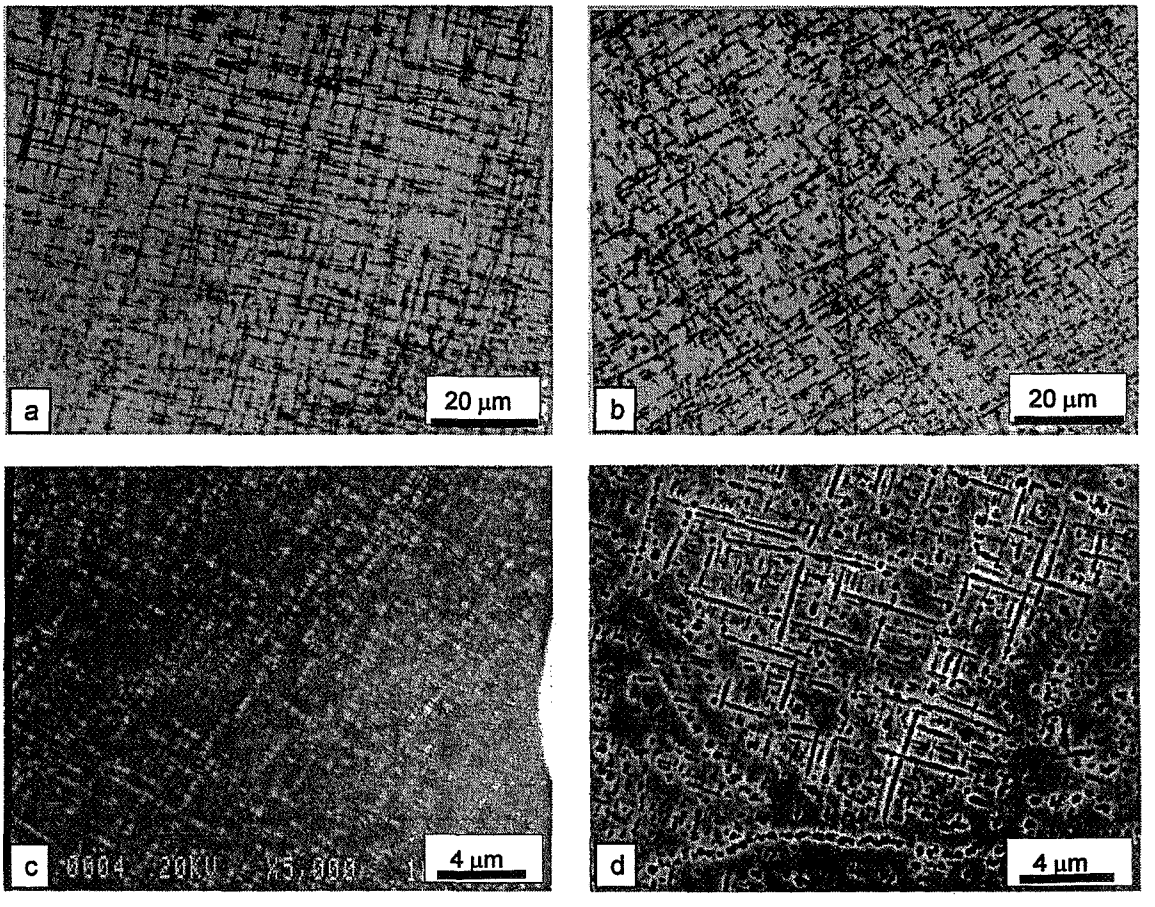

Figure 2. Optical micrographs of etched (a) D219 (Ni-45.4Al-0.57Hf-0.2Ga-5.4Ti-0.32Si) and (b) D218 (Ni-49.7Al-0.51Hf-0.12Ga-1.0Ti-.15Si) and SEM micrographs of A-26 (Ni-42.4Al-0.77Hf-0.1Ga-4.0Ti-0.9Cr-0.32Si) (c) unetched and (d) etched, before testing.

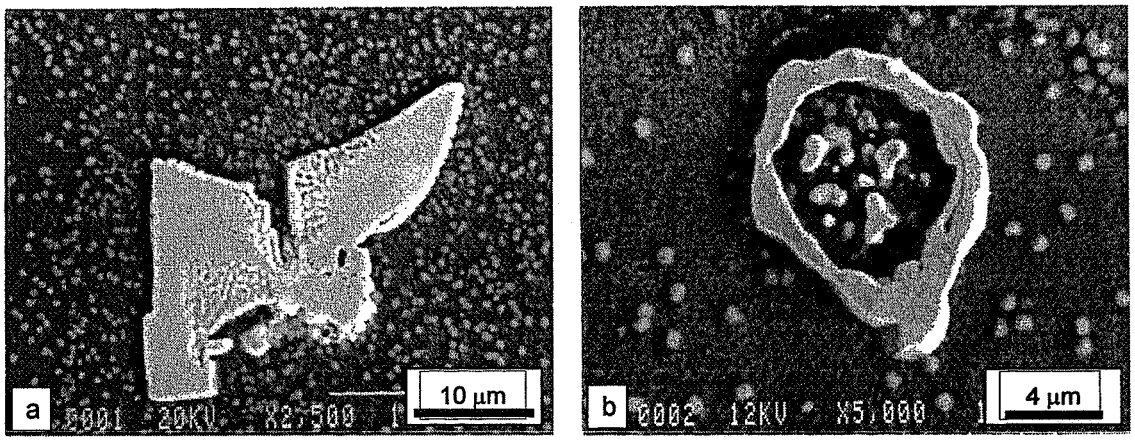

Figure 3. SEM micrographs of a (a) carbide and (b) oxide in etched D218 (Ni-49.7Al-0.51Hf-0.2Ga-1.0Ti-0.15Si) before testing.

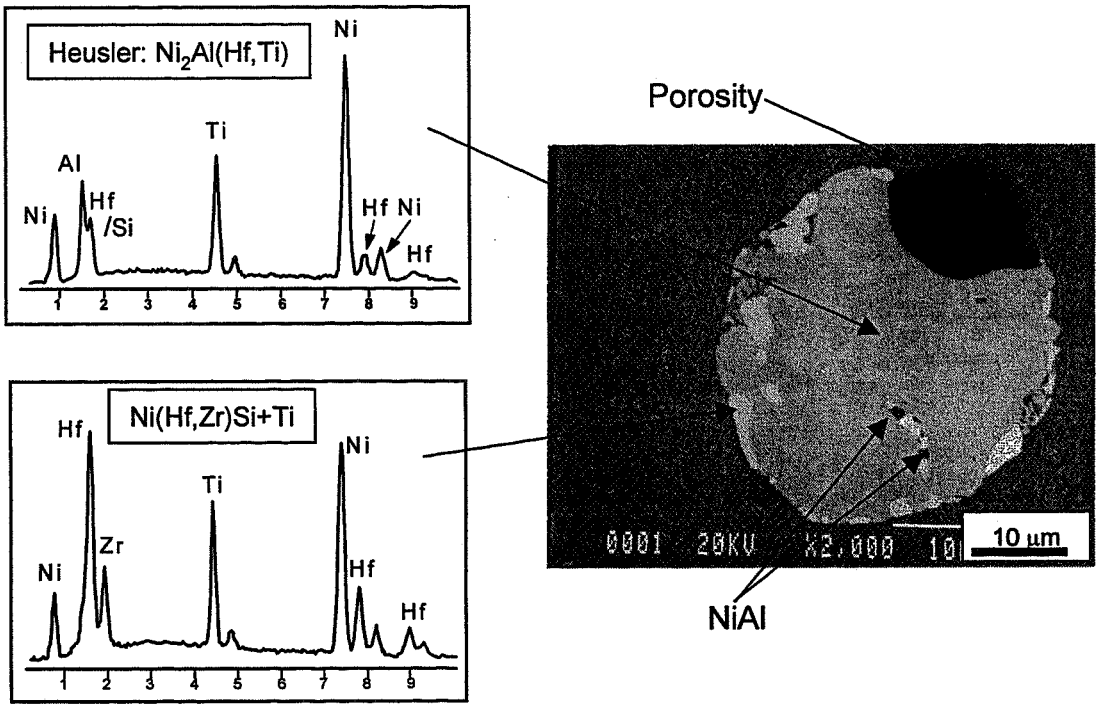

Figure 4. Example of three-phase eutectic particle of primarily Heusler phase remaining in interdendritic regions (Ni-42.4Al-0.77Hf-0.13Ga-4.0Ti-0.9Cr-0.32Si) before testing.

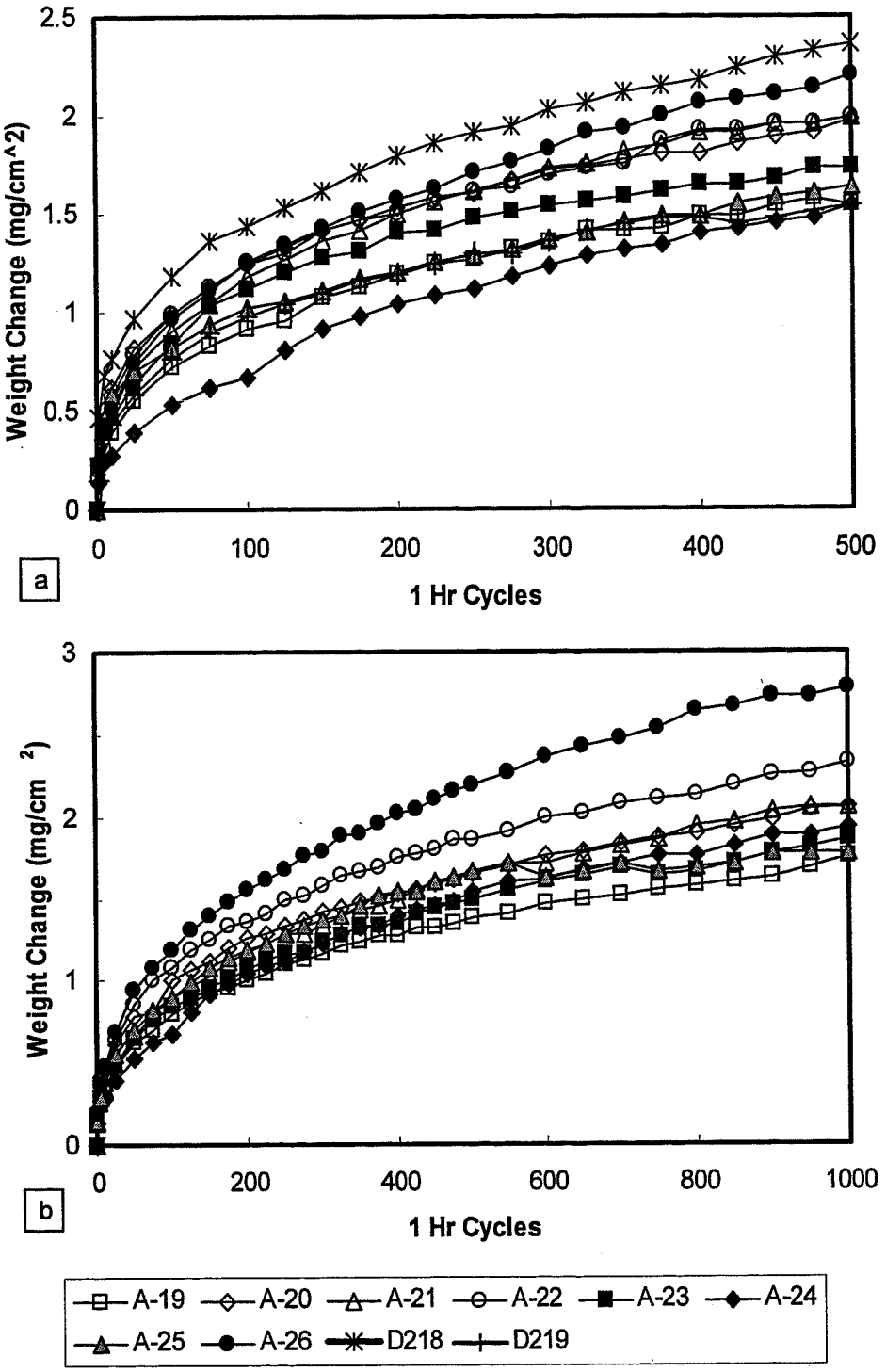

Figure 5. Weight change through (a) 500 and (b) 1000 1-hr cycles for each of the alloys. Weight change for binary NiAl and NiAl-Zr (reference 9) shown in (b) for comparison.

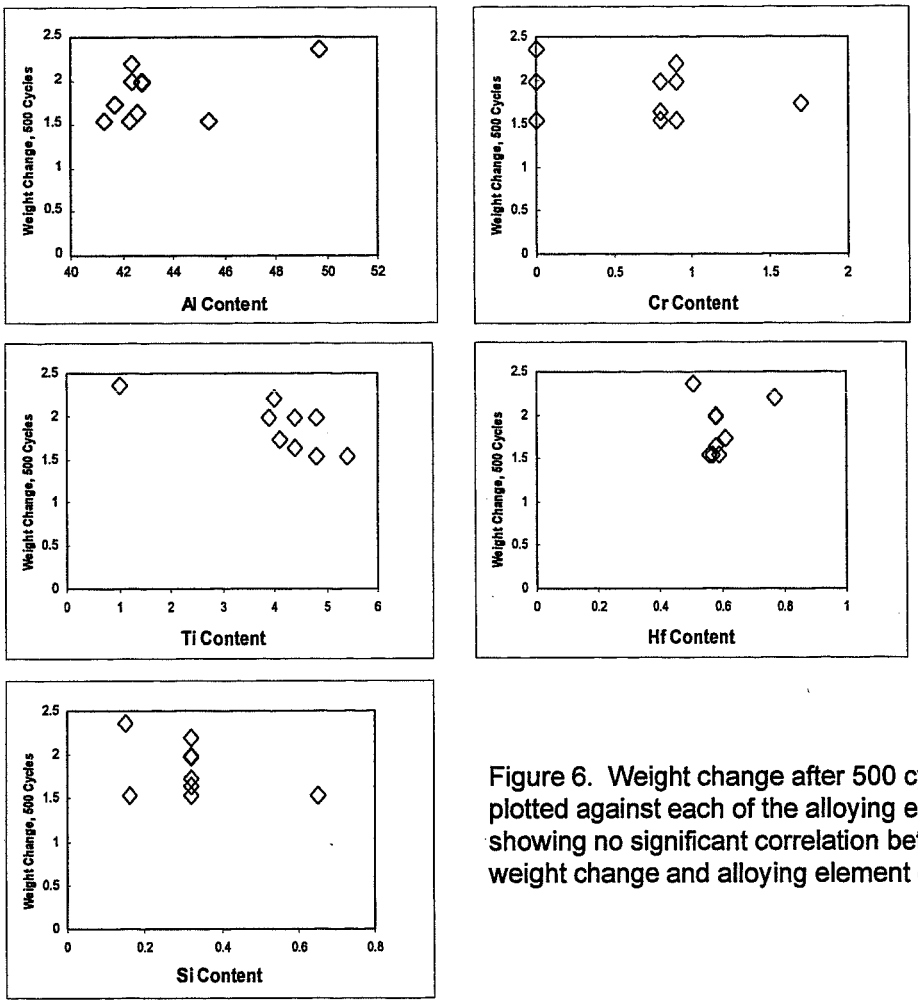

Figure 6. Weight change after 500 cycles plotted against each of the alloying elements showing no significant correlation between weight change and alloying element content.

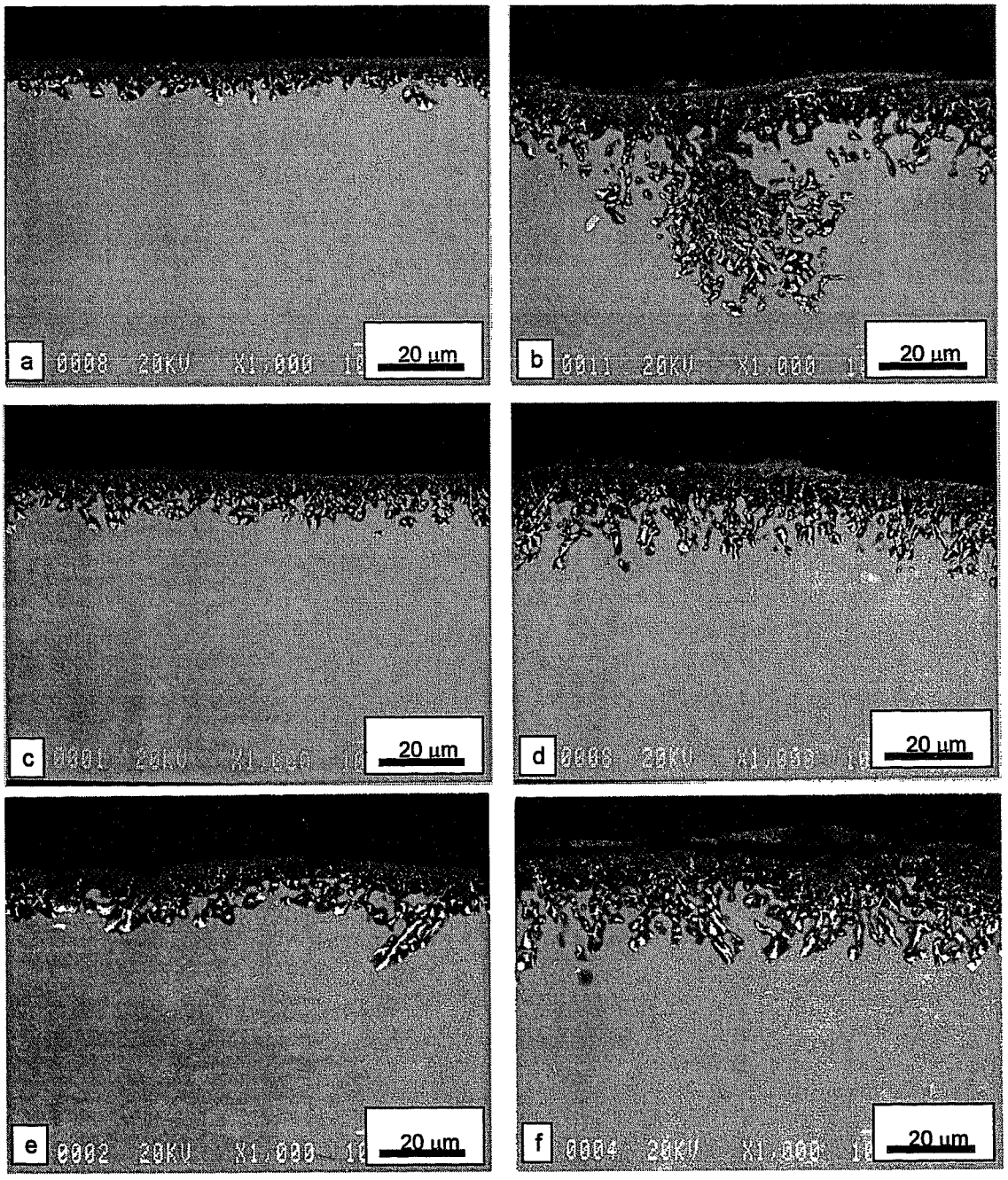

Figure 7. Typical oxide scale on (a,b) D219 (Ni-45.4Al-0.57Hf-0.2Ga-5.4Ti-0.32Si after 500 cycles, and on (c,d) A-26 (Ni-42.4Al-0.77Hf-0.13Ga-4.0Ti-0.9Cr-0.32Si) after 500 and (e,f) after 1000 cycles.

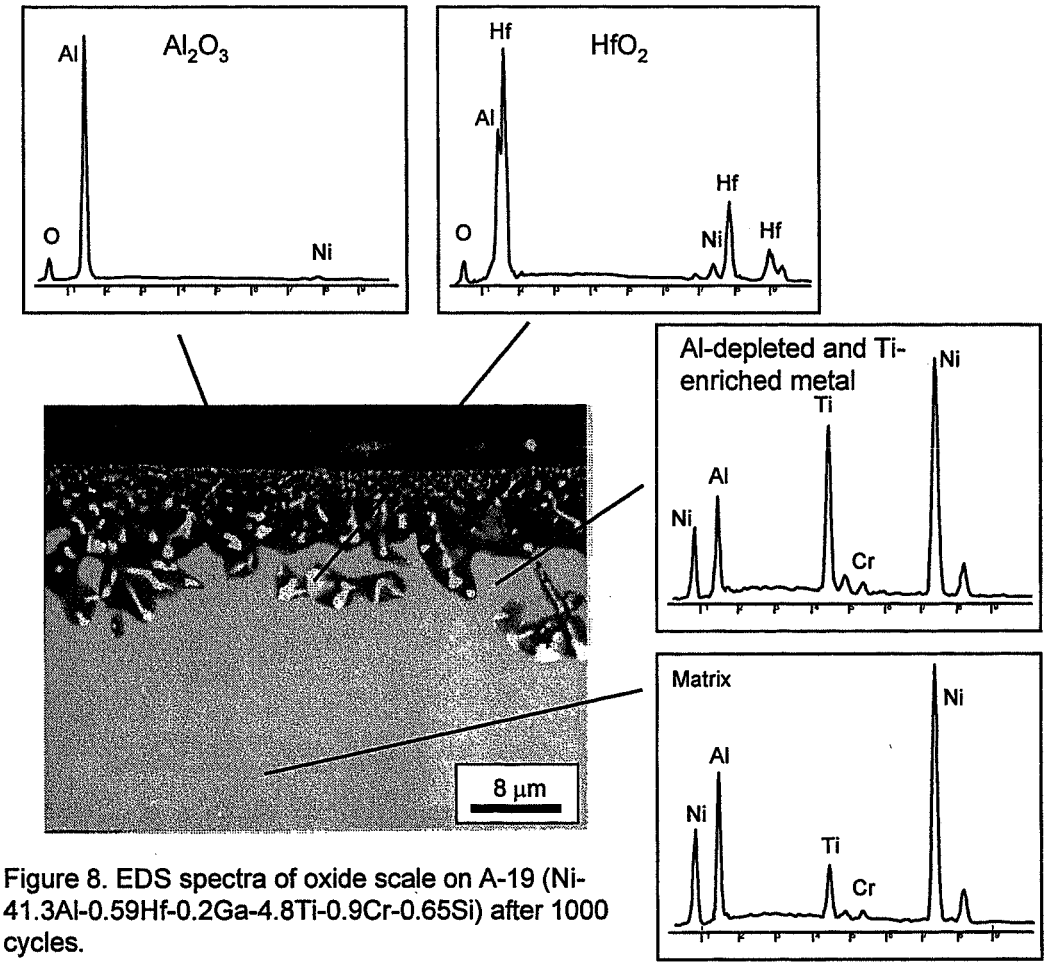

Figure 8. EDS spectra of oxide scale on A-19 (Ni-41.3Al-0.59Hf-0.2Ga-4.8Ti-0.9Cr-0.65Si) after 1000 cycles.

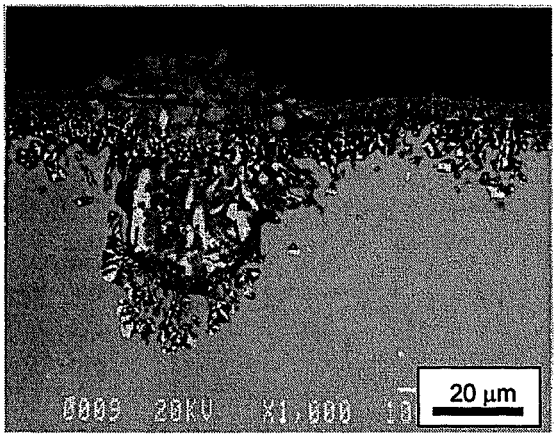

Figure 9. Oxidation of one of the three-phase eutectic particles at the surface on D219 (Ni-45.4Al-0.57Hf-0.2Ga-5.4Ti-0.32Si) after 500 cycles.

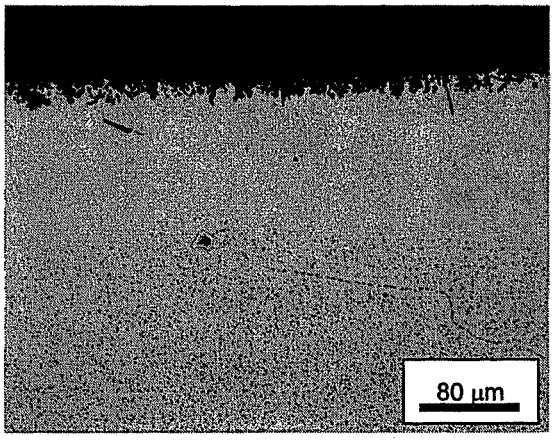

Figure 10. Depletion of the Heusler phase in A-26 (Ni-42.4Al-0.77Hf-0.1Ga-4.0Ti-0.9Cr-0.32Si) after 1000 cycles.